Inhibition of Cytosolic Phospholipase A$_2$ Has Neuroprotective Effects on Motoneuron and Muscle Atrophy after Spinal Cord Injury

Nai-Kui Liu,[1] James S. Byers,[2] Tom Lam,[3] Qing-Bo Lu,[1] Dale R. Sengelaub,[2] and Xiao-Ming Xu[1]

Abstract

Surviving motoneurons undergo dendritic atrophy after spinal cord injury (SCI), suggesting an important therapeutic target for neuroprotective strategies to improve recovery of function after SCI. Our previous studies showed that cytosolic phospholipase A$_2$ (PLA$_2$) may play an important role in the pathogenesis of SCI. In the present study, we investigated whether blocking cytosolic PLA$_2$ (cPLA$_2$) pharmacologically with arachidonyl trifluoromethyl ketone (ATK) or genetically using cPLA$_2$ knockout (KO) mice attenuates motoneuron atrophy after SCI. C57BL/6 mice received either sham or contusive SCI at the T10 level. At 30 min after SCI, mice were treated with ATK or vehicle. Four weeks later, motoneurons innervating the vastus lateralis muscle of the quadriceps were labeled with cholera toxin-conjugated horseradish peroxidase, and dendritic arbors were reconstructed in three dimensions. Soma volume, motoneuron number, lesion volume, and tissue sparing were also assessed, as were muscle weight, fiber cross-sectional area, and motor endplate size and density. ATK administration reduced percent lesion volume and increased percent volume of spared white matter, compared to the vehicle-treated control animals. SCI with or without ATK treatment had no effect on the number or soma volume of quadriceps motoneurons. However, SCI resulted in a decrease in dendritic length of quadriceps motoneurons in untreated animals, and this decrease was completely prevented by treatment with ATK. Similarly, vastus lateralis muscle weights of untreated SCI animals were smaller than those of sham surgery controls, and these reductions were prevented by ATK treatment. No effects on fiber cross-sectional areas, motor endplate area, or density were observed across treatment groups. Remarkably, genetically deleting cPLA$_2$ in cPLA$_2$ KO mice attenuated dendritic atrophy after SCI. These findings suggest that, after SCI, cord tissue damage and regressive changes in motoneuron and muscle morphology can be reduced by inhibition of cPLA$_2$, further supporting a role for cPLA$_2$ as a neurotherapeutic target for SCI treatment.

Key words: atrophy; cPLA$_2$; dendrites; morphology; neuroprotection

Introduction

TRAUMATIC SPINAL CORD INJURIES (SCIs) are prevalent in the United States, where more than 11,000 people per year survive a SCI. Of these, approximately 45% suffer from spinal motoneuron lesions, and this number rises to approximately 95% for those with lumbar or sacral injuries.[1] The pathophysiology of SCI involves both immediate and secondary effects. After the initial trauma, a protracted period of progressive damage occurs, causing spreading of the lesion and further segmental destruction. A variety of mechanisms contribute to this progressive secondary injury, including excitotoxicity,[2] free radical generation,[3] and inflammation,[4] resulting in the death of motoneurons, interneurons, and glial cells at the lesion site. Caudal to the lesion, surviving motoneurons

respond to injury with marked dendritic retraction.[5] This secondary dendritic atrophy is likely responsible for at least some of the movement deficits and reduces the excitability of the remaining motoneurons.[6] The target musculature of these motoneurons is also affected, with reductions in weight and fiber cross-sectional fiber diameter.[5]

Given that we currently lack the technology to replace dead motoneurons, developing the ability to protect motoneurons from injury-induced cell death and/or surviving motoneurons from secondary atrophy is an important goal. Our previous studies suggest that activation of phospholipase A$_2$ (PLA$_2$) may play an important role in mediating the secondary effects of SCI.[7,8] The hydrolysis of membrane phospholipids by PLA$_2$ is a rate-limiting step for generation of proinflammatory mediators, such as eicosanoids and

[1]Spinal Cord and Brain Injury Research Group, Stark Neurosciences Research Institute, Department of Neurological Surgery and Goodman Campbell Brain and Spine, Indiana University School of Medicine, Indianapolis, Indiana, USA.
[2]Program in Neuroscience and Department of Psychological and Brain Sciences, Indiana University, Bloomington, Indiana, USA.
[3]Indiana University School of Medicine, Bloomington, Indiana, USA.

platelet-activating factor (PAF).[9–11] Eicosanoids and PAF are well-known mediators of inflammation and tissue injury and have been implicated in pathological states of numerous acute and chronic neurological disorders.[9,10,12] SCI significantly increased total PLA_2 activation and expression of cytosolic PLA_2 ($cPLA_2$).[8] Further, expression of phosphorylated $cPLA_2$, a marker for $cPLA_2$ activation, was increased postinjury in injured axons, glial cells, and neurons.[13] Administration of exogenous PLA_2 or melittin, a potent activator of endogenous PLA_2, resulted in cultured spinal neuronal death in a dose-dependent manner.[8] Importantly, such PLA_2- or melittin-mediated neuronal death could be significantly reversed by inhibiting PLA_2,[7,8] and inhibition of PLA_2 improved behavioral recovery after SCI in mice.[13] Thus, blocking PLA_2 activation may represent a novel strategy to reduce multiple damaging processes in the course of secondary SCI that leads to motoneuron atrophy.

To date, more than 27 isoforms of PLA_2 have been found in the mammalian system, which can be classified into three major categories: secretory PLA_2 ($sPLA_2$), $cPLA_2$, and Ca^{2+}-independent PLA_2 ($iPLA_2$).[11,14] Of these, $cPLA_2$ is the most important PLA_2 isozyme and has been implicated as an effector in receptor-mediated release of arachidonic acid (AA) and exhibits strong preference for deacylation of AA over other fatty acids (FAs).[9,15] Because $cPLA_2$ activation mediates semaphorin 3A (Sema3A)-induced growth cone collapse,[16,17] it is possible that $cPLA_2$ activation is involved in dendritic atrophy after SCI. However, no studies to date have examined whether $cPLA_2$ has a role in motoneuron atrophy. In this study, we investigated the effects of $cPLA_2$ inhibition on spinal motoneurons and their target musculature after SCI.

Methods

Female C57BL/6 mice (12 weeks) were purchased from The Jackson Laboratory (Bar Harbor, ME). Female $cPLA_2^{-/-}$ mice and wild-type (WT) littermates (12 weeks) generated from heterozygous breeding pairs at Indiana University School of Medicine Laboratory Animal Resource Center (Indianapolis, IN) were used in this study. Mice were maintained on a 12:12 light/dark cycle with food and water freely available. A total of 38 animals were used for the study and were divided into five groups: sham-operated ($n=6$); SCI ($n=8$); SCI + ATK (arachidonyl trifluoromethyl ketone; $n=8$); WT SCI ($n=8$); and $cPLA_2$ knockout (KO) SCI ($n=8$). All surgical interventions and postoperative animal care were performed in accord with the Guide for the Care and Use of Laboratory Animals (National Research Council) and were approved by the Indiana University Institutional Animal Care and Use Committee.

Spinal cord contusion and treatment

Mice were anesthetized by an intraperitoneal (i.p.) injection of 2.5% Avertin (2,2,2-tribromo-ethanol, 0.15 mL/10 g body weight; Sigma-Aldrich, St Louis, MO). A T10 laminectomy was performed to expose the underlying thoracic spinal cord segment(s), and animals received a (60-kDyne) contusion injury using an Infinity Horizon impactor. Spinal cord injury at the T10 vertebra (T12–T13 spinal cord)[18] was intended to preserve central pattern generators at L1–L2 required for locomotor function, as well as the relevant motoneurons for our analysis. Sham control animals received laminectomy only. After injury, muscles and skin were closed in layers, and animals were placed in a temperature- and humidity-controlled chamber overnight. Manual bladder expression was carried out at least three times daily until reflex bladder emptying was established.

After contusion injury, mice were treated with a potent, selective slow-binding inhibitor of $cPLA_2$, ATK.[19] ATK (Cayman Chemi-

cals, Ann Arbor MI) was injected intravenously (50 μL of 4 mM) at 30 min after injury; mice received additional ATK injections administered i.p. (200 μL of 4 mM) on every other day up to 2 weeks postinjury; another group of SCI animals received vehicle injections. The dose and treatment regimens were selected based on our previous publication[13] and a previously published report.[20] Animals were allowed to survive for 4 weeks after SCI, a length of time sufficient to observe induced effects on motoneuron morphology.[6,21–23] An additional group of age-matched, sham-injured (laminectomy-only) females served as normal controls.

Injection of horseradish peroxidase conjugated to cholera toxin B subunit

Four weeks after injury, animals were reanesthetized, and the left vastus lateralis muscle of the quadriceps was exposed and injected with horseradish peroxidase conjugated to the cholera toxin B subunit (BHRP; 0.5 μL, 0.2%; List Biological, Inc., Campbell, CA). BHRP labeling permits population-level quantitative analysis of motoneuron somal and dendritic morphologies.[24,25] Forty-eight hours after BHRP injection, a period that ensures optimal labeling of motoneurons,[24,25] animals were weighed and received a lethal dose of Nembutal (60 mg/kg, i.p.) and were then perfused intracardially with saline, followed by cold fixative (1% paraformaldehyde/1.25% glutaraldehyde).

Tissue processing, histology, and lesion assessments

A 12-mm thoracic spinal cord segment, including the lesion, was removed, postfixed overnight in the same fixative as used for perfusion, and transferred to sucrose phosphate buffer (30% w/v; pH 7.4). Thoracic segments were then embedded in gelatin, frozen, and sectioned transversely at 40 μm; alternate sections were collected into two series and mounted on gelatin-coated slides. One series was stained with cresyl violet and eosin for assessing lesion and spared tissue volume. Cross-sectional areas of lesion or spared white (WM) and gray matter (GM) for each animal were measured in sections located 240 μm apart and spanning the entire rostrocaudal extent of the lesion using a video-based morphometry system (Stereo Investigator; MBF Bioscience, Williston, VT) at a final magnification of 202×. An unbiased estimation of the percentage of spared tissue was calculated using Cavalieri's method.[26] Total volume of spared WM and GM was calculated by summing their individual subvolumes.[27] Individual subvolumes of spared tissue were calculated by multiplying the cross-sectional area $A \times d$, where d represents the distance between sections (240 μm). The percent total volume of spared WM and GM was calculated by dividing the total volume of spared WM and GM by the total tissue volume of the corresponding region (100×), respectively. Estimation of total and percent total lesion volume was determined using identical procedures. The remaining series of thoracic sections were stained for myelin using Luxol fast blue (LFB), as described previously.[7] The lesion area and total spinal cord area were outlined from a section through the lesion epicenter and sections located either 240 μm rostral or caudal to the epicenter using Stereo Investigator. The percent lesion area was determined by dividing the lesion area by the spinal cord area from the same section.

Motoneuron morphology and quantification

The vastus lateralis muscle is innervated by motoneurons located in column 3 of the lateral motor column in the L2 spinal segment.[28–30] After perfusion, the lumbar portion of the spinal cord of each animal was removed, postfixed for 5 h in the same fixative as used for perfusion, and then transferred to sucrose phosphate buffer (10% w/v; pH 7.4) overnight for cryoprotection. Spinal cords were then embedded in gelatin, frozen, and sectioned transversely at 40 μm; all sections were collected into four alternate series. One

series was stained with thionin for use in cell counts. For visualization of BHRP, the three remaining series were immediately reacted using a modified tetramethyl benzidine protocol,[5] mounted on gelatin-coated slides, and counterstained with thionin.

Motoneurons innervating the quadriceps muscles do not form a discrete nucleus, but instead are contained within the large continuous populations of motoneurons located within the lateral motor column. Thus, to identify the appropriate area within the lateral motor column for motoneuron counts in the unreacted series, we used a method similar to that of Little and colleagues.[6] Briefly, for each animal, the range of sections in which motoneurons labeled with BHRP after injection into the vastus lateralis muscle were present in the reacted series was identified, and then motoneuron counts were performed in the appropriate matching sections in the unreacted series. For each animal, estimates of the total number of motoneurons in the left and right lateral motor columns were obtained using the optical disector method, as previously described.[6] Counts were made at 937.5× under brightfield illumination. Motoneurons are easily recognizable as large, darkly staining, multipolar cells. A counting frame ($110 \times 80 \, \mu$m) was moved systematically throughout an area of each ventral horn (approximately $350 \times 350 \, \mu$m, defined by the actual distribution of BHRP-labeled somata from all of the animals used in the study) in each section within the identified range. Only motoneurons in which there was a clear nucleus and nucleolus were counted, provided they did not contact the forbidden lines of the counting frame; motoneuron nucleoli were counted as they appeared while focusing through the z-axis, and nucleoli in the first focal plane (i.e., "tops") were excluded to avoid double counting. Motoneuron counts were derived from a mean of 5.33 sections spaced $480 \, \mu$m apart and distributed uniformly through the entire rostrocaudal extent of the quadriceps motoneuron pool range. Cell counts for each animal were corrected for the proportion of sections sampled.

Using similar methods, the number of BHRP-labeled motoneurons was assessed in all sections of the reacted series through the entire rostrocaudal extent of their distribution for all animals. Counts of labeled quadriceps motoneurons were made under brightfield illumination, where somata could be visualized and cytoplasmic inclusion of BHRP reaction product confirmed.

Soma volume

The volume of quadriceps motoneuron somata was assessed in at least one set of alternate sections ($160 \, \mu$m apart) using the nucleator method.[31] A set of four rays emanating from a point randomly chosen within each BHRP-labeled motoneuron soma was drawn and oriented randomly. Soma volumes of an average of 28.1 motoneurons were measured for each animal using Stereo Investigator at a final magnification of 780×. Soma volumes within each animal were then averaged for statistical analysis.

Dendritic length

For each animal, dendritic lengths in a single representative set of alternate sections were measured under darkfield illumination. Beginning with the first section in which BHRP-labeled fibers were present, labeling through the entire rostrocaudal extent of the quadriceps motoneuron dendritic field was assessed in every third section ($480 \, \mu$m apart) in three dimensions using a computer-based morphometry system (Neurolucida; MBF Bioscience) at a final magnification of 250×. Average dendritic length per labeled motoneuron was estimated by summing the measured dendritic lengths of the series of sections, multiplying by three to correct for sampling, then dividing by the total number of labeled motoneurons in that series. This method does not attempt to assess the actual total dendritic length of labeled motoneurons,[32] but has been shown to be a sensitive, reliable indicator of changes in dendritic morphology in normal development,[24,33,34] after changes in dendritic interactions[33] and afferent input,[35–37] as well as after injury.[6,21–23,38]

Dendritic distribution

To assess potential redistributions of dendrites across treatment groups, for each animal, the composite dendritic arbor created in the length analysis was divided using a set of axes oriented radially around the center of the collective labeled somata. These axes divided the spinal cord into 12 bins of 30 degrees each. The portion of each animal's dendritic arbor per labeled motoneuron contained within each location was then determined. This method provides a sensitive measure of dendritic redistribution in response to changes in dendritic interactions[33] and afferent input.[35,36]

Dendritic extent

Comparability of BHRP labeling across groups was assessed by quantifying both the rostrocaudal and the radial extent of quadriceps motoneuron dendritic arbors. The rostrocaudal extent of the dendritic arbor was determined by recording the rostrocaudal distance spanned by quadriceps motoneuron dendrites for each animal. The maximal radial extent of the arbor in the transverse plane was also measured for each animal, using a set of axes oriented radially around the center of the collective labeled somata. These axes divided the spinal cord into 12 bins of 30 degrees each. For each bin, the linear distance between the center of the quadriceps motor pool and the most distal BHRP-filled process was measured. Radial dendritic extent is independent of overall dendritic length and reflects the maximal linear distance (in the transverse plane) of BHRP transport to the most distal dendritic processes.

Muscle fiber and motor endplate morphology

The right vastus lateralis muscles were removed immediately after perfusion and weighed. Muscles were then postfixed overnight in the same fixative as used for perfusion and then transferred to sucrose phosphate buffer (10% w/v; pH 7.4). Muscles were then rinsed in distilled water, blocked into proximal and distal segments, and flash-frozen in 2-methylbutane. Muscle segments were then sectioned ($45 \, \mu$m) either transversely (for examination of muscle fiber cross-sectional area) or longitudinally (for examination of motor endplate area and density) on a cryostat at $-20°$C and thaw-mounted onto glass slides. Muscle fiber cross-sectional area was assessed after staining with Milligan's trichrome stain. Motor endplate size and density were assessed after staining for acetylcholinesterase using Roots-Karnovsky's method.[39] Cross-sectional muscle fiber area and motor endplate size were measured under brightfield illumination using Stereo Investigator. To obtain accurate measures of motor endplate size, only *en face* profiles were traced. An average of 32.5 muscle fibers and 30.0 endplates were measured for each animal at a final magnification of 510×. The number of motor endplates per muscle fiber was estimated by counting the number of muscle fibers and endplates in a grid (1×1 mm), randomly placed on the muscle section (one sample field per section, five muscle sections per animal). An average of 139.8 muscle fibers per animal was examined. Fiber and endplate areas within each animal were then averaged for statistical analysis.

Statistical analysis

All data are presented as mean ± standard error of the mean (SEM) and were analyzed by *t*-tests or analyses of variance (ANOVA; one way, two way, or repeated measures, as appropriate) followed by post-hoc analyses using Fisher's least significant difference (LSD). Digital light micrographs were obtained using an MDS 290 digital camera system (Eastman Kodak Company, Rochester, NY). Brightness and contrast of these images were adjusted in Adobe Photoshop (Adobe Systems, San Jose, CA).
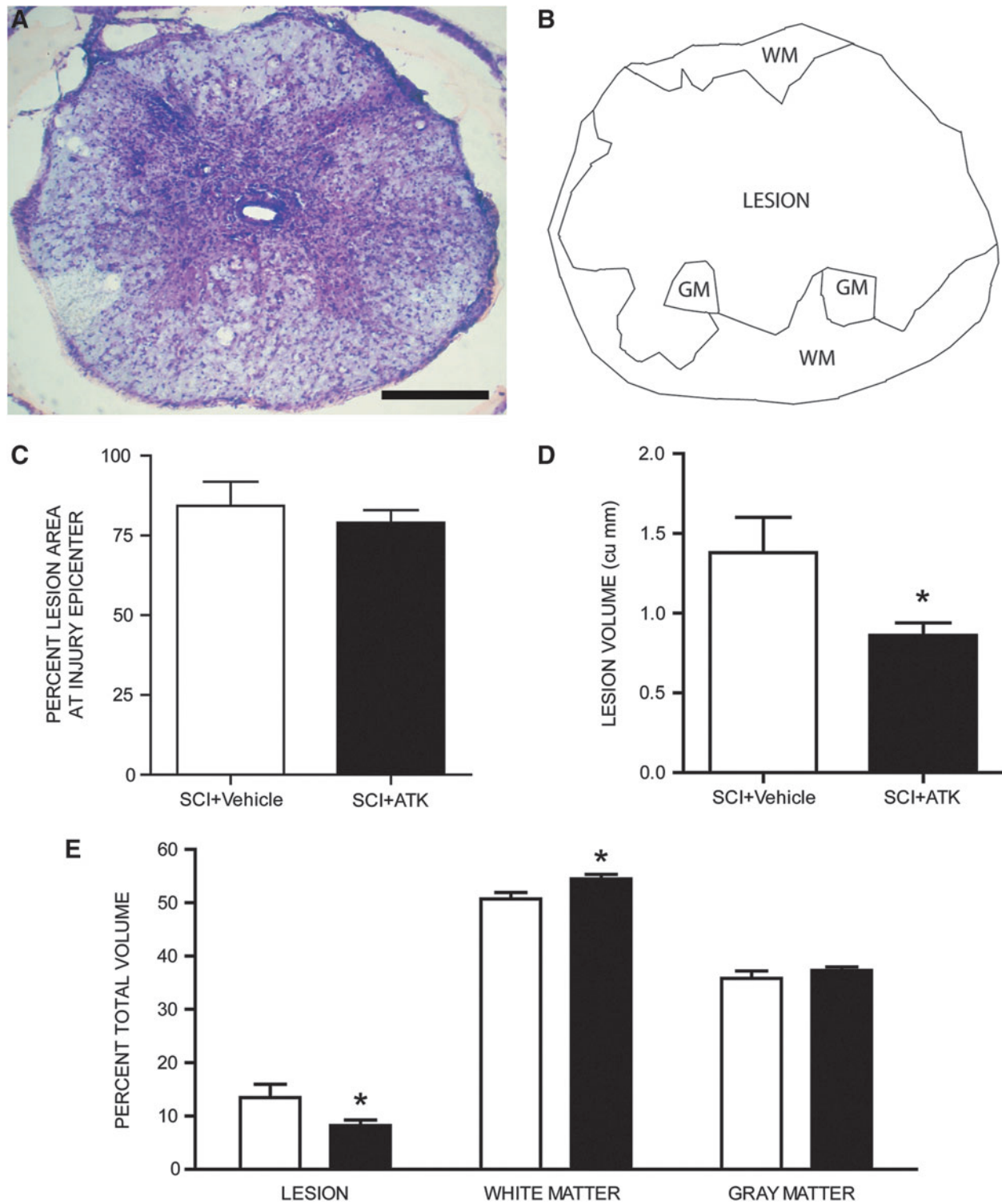
FIG. 1. Histological and stereological analysis of spinal cord spared tissue and lesion volume after contusive spinal cord injury (SCI) with or without arachidonyl trifluoromethyl ketone (ATK) treatment. (**A**) Representative section near the lesion epicenter stained with cresyl violet and eosin, showing a large centrally located lesion with areas of spared gray (GM) and white matter (WM). (**B**) Neurolucida drawing from the same section showing the lesion area, residual WM, and spared GM. (**C**) Percentage of lesion area at injury epicenter did not differ across injured animals that were either untreated (SCI) or treated with ATK (SCI+ATK). However, lesion volumes (**D**) and percent total volumes (**E**) of lesion and spared WMs differed across groups. Scale bar, 250 μm. Color image is available online.

Results

Lesion volume and white matter sparing

Contusive SCI resulted in large lesion with thin rims of spared tissue (Fig. 1A,B). In both SCI groups, faint staining with LFB indicated that contusion injury resulted in areas of demyelination immediately surrounding the lesion. Measurements of the percent lesion area in LFB-stained sections indicated that treatment with ATK had no effect on percent lesion area at the injury epicenter, with the lesion occupying an average of 81.68% of the total cord area ($t[12] = -0.652$, not significant [n.s.]; Fig. 1C). In contrast, lesion volumes in vehicle-treated animals ($1.38 \pm 0.22\,\mathrm{mm}^3$; mean $\pm$SEM) were significantly larger than those of ATK-treated animals ($0.86 \pm 0.08\,\mathrm{mm}^3$; $F_{(1,12)} = 6.25$; $p < 0.03$; Fig. 1D). To correct for changes in spinal cord contour after spinal cord contusion, percent lesion volume was also determined. As for total lesion volume, ATK treatment had a significant effect on percent lesion volume (SCI + vehicle, $13.48 \pm 2.52\%$; SCI + ATK, $8.20 \pm 1.07\%$), percent volume of spared WM (SCI + vehicle, $50.70 \pm 1.22\%$; SCI + ATK, $54.48 \pm 0.86\%$), and percent volume of spared GM (SCI + vehicle, $35.81 \pm 1.43\%$; SCI + ATK, $37.32 \pm 0.65\%$; $F_{(1, 24)} = 4.31$; $p < 0.03$; Fig. 1E). Importantly, despite the large size of the lesions, they did not extend into the L2 level and thus did not compromise the quadriceps motoneuron populations directly.

Motoneuron counts

In sham animals, the number of motoneurons within the identified quadriceps range averaged 727.50 ($\pm$100.09). Contusive SCI with or without ATK treatment had no effect on the number of quadriceps motoneurons (SCI + vehicle, 668.00 ± 72.11; SCI + ATK, 708.00 ± 108.43; $F_{(2, 19)} = 0.09$, n.s.).

Motoneuron morphometry

Injection of BHRP into the left vastus lateralis successfully labeled ipsilateral quadriceps motoneurons in all groups (Fig. 2). Labeled motoneurons were located in the lateral motor column in the L2 spinal segment.[6,28] Dendritic arbors were strictly unilateral, with extensive ramification along the ventrolateral edges of the GM and in the lateral funiculus, as well as throughout the ventral horn. An average of 73.92 ± 6.60 motoneurons per animal were labeled with BHRP and did not differ by group ($F_{(2,18)} = 0.24$, n.s.).

Soma volume

In sham animals, quadriceps motoneuron somata were typical in size ($12,539.46 \pm 644.53\,\mu\mathrm{m}^3$) and did not differ from those of SCI + vehicle ($12,561.79 \pm 378.75\,\mu\mathrm{m}^3$) or SCI + ATK animals ($11,926.33 \pm 690.53\,\mu\mathrm{m}^3$; $F_{(2,19)} = 0.35$, n.s.).

Dendritic length

After contusion injury, quadriceps motoneurons underwent marked dendritic atrophy. Dendritic length decreased by 28.3% ($2870.71 \pm 215.17\,\mu\mathrm{m}$ in SCI + vehicle animals, compared to $4002.23 \pm 193.64\,\mu\mathrm{m}$ for sham animals; LSD, $p < 0.05$; overall test for effect of group on arbor per cell $F_{(2,18)} = 3.68$; $p < 0.05$; Fig. 3A). However, treatment with ATK attenuated SCI-induced dendritic atrophy: Dendritic lengths in SCI + ATK animals ($4210.34 \pm 550.30\,\mu\mathrm{m}$) were 46.7% longer than those of SCI + vehicle animals (LSD, $p < 0.03$) and did not differ from those of sham animals (LSD, n.s.; Fig. 3A).

Dendritic length per bin was nonuniform across radial bins, and a repeated-measures ANOVA revealed a significant effect of radial
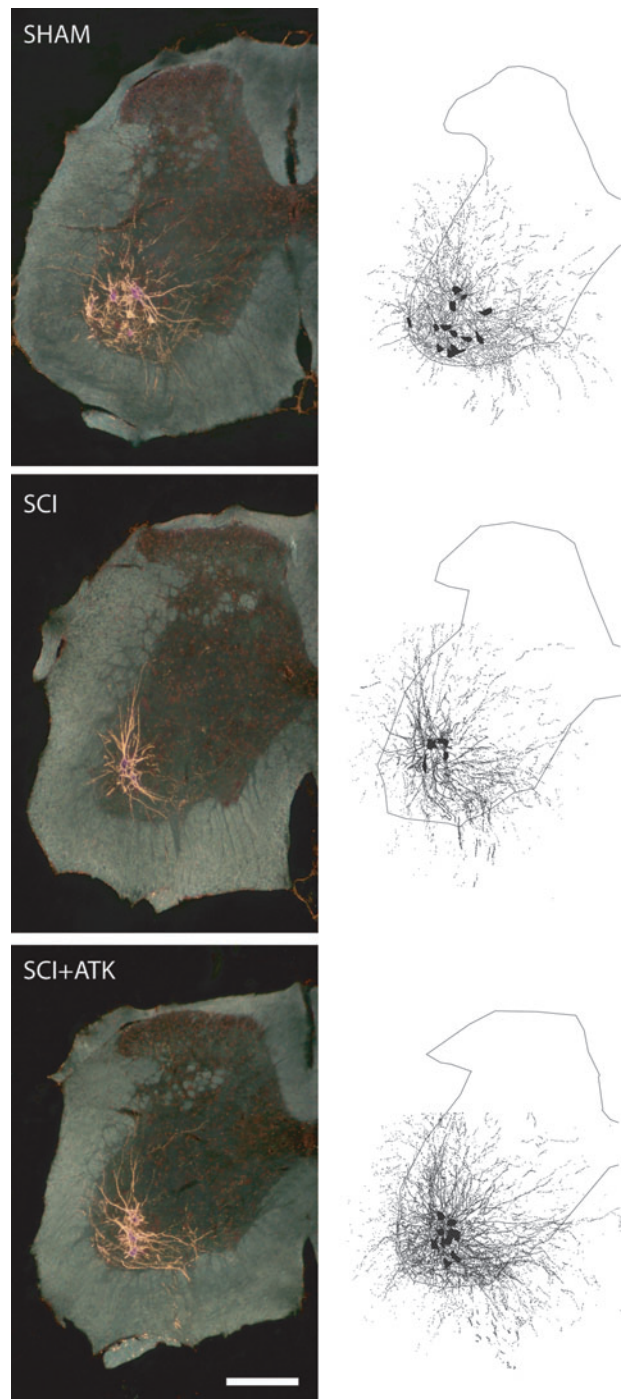

FIG. 2. (Left) Darkfield digital micrographs of transverse hemisections through the lumbar spinal cords of a sham animal (top), an injured animal treated with vehicle (spinal cord injury [SCI] + vehicle, middle), and an arachidonyl trifluoromethyl ketone (ATK)-treated injured animal (SCI + ATK, bottom), after injection of horseradish peroxidase conjugated to the cholera toxin B subunit (BHRP) into the left vastus lateralis muscle. (Right) Computer-generated composites of BHRP-labeled somata and processes drawn at 480-μm intervals through the entire rostrocaudal extent of the quadriceps motor pool; these composites were selected because they are representative of their respective group average dendritic lengths. Scale bar, 250 μm. Color image is available online.
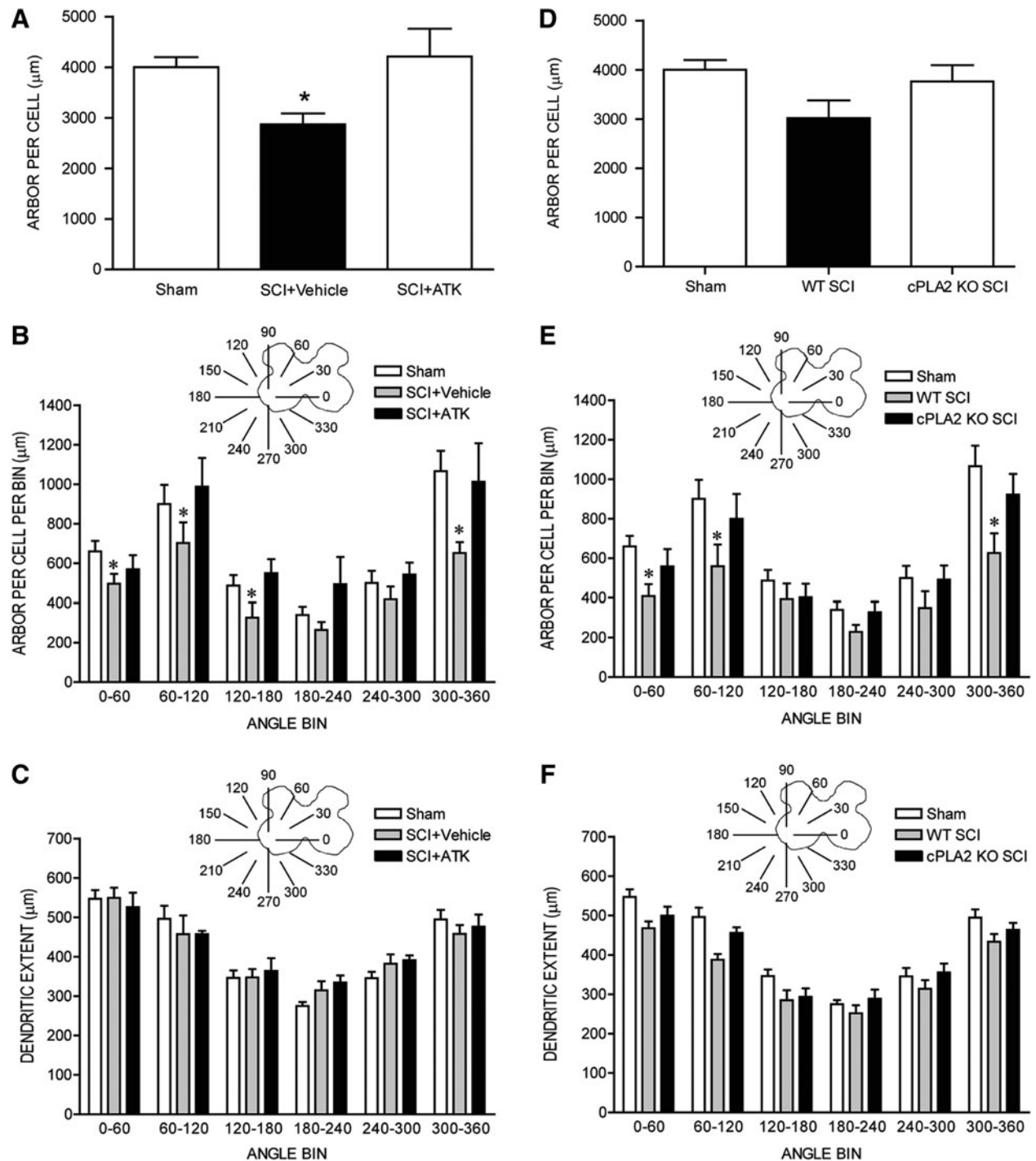
FIG. 3. (**A**) Dendritic lengths of quadriceps motoneurons after spinal cord injury (SCI). After contusion injury, surviving quadriceps motoneurons lost over 28% of their dendritic length. Treatment with arachidonyl trifluoromethyl ketone (ATK) attenuated this dendritic atrophy. *Significantly different from sham animals. Inset: Drawing of spinal gray matter divided into radial sectors for measure of quadriceps motoneuron dendritic distribution (**B** and **E**) and radial dendritic extent (**C** and **F**). (B) Length per radial bin of quadriceps dendrites of sham animals (unfilled bars) and injured animals that were either untreated (SCI + vehicle, gray bars) or treated with ATK (SCI + ATK, black bars). For graphic purposes, dendritic length measures have been collapsed into six bins of 60 degrees each. Quadriceps motoneuron dendritic arbors display a nonuniform distribution, with the majority of the arbor located between 300 and 120 degrees. After contusion injury, surviving quadriceps motoneurons in untreated animals had reduced dendritic lengths throughout the radial distribution. Treatment with ATK attenuated these reductions. *Significantly different from sham animals. (C) Radial extents of quadriceps dendrites of sham animals (unfilled bars) and injured animals that were either untreated (SCI + vehicle, gray bars) or treated with ATK (SCI + ATK, black bars). For graphic purposes, dendritic extent measures have been collapsed into six bins of 60 degrees each. After contusion injury, extent measures of surviving quadriceps motoneurons in SCI + vehicle and SCI + ATK animals did not differ from those of sham animals. (**D**) Dendritic lengths of quadriceps motoneurons of sham animals and injured animals that were either wild type (WT) or cPLA$_2$ knockout (KO). Genetic deletion of cPLA$_2$ attenuated SCI-induced dendritic atrophy. (E) Length per radial bin of quadriceps dendrites of sham animals (unfilled bars) and injured animals that were either WT (gray bars) or cPLA$_2$ KO mice (black bars). There is a significant effect of radial dendritic location. (F) Radial extents of quadriceps dendrites of sham animals (unfilled bars) and injured animals that were either WT (gray bars) or cPLA$_2$ KO mice (black bars). Radial dendritic extent did not differ across groups. cPLA$_2$, cytosolic phospholipase A$_2$.

location ($F_{(11,198)} = 21.76$; $p < 0.0001$; Fig. 3B). Consistent with the results of the arbor per-cell analysis, there was also a significant effect of group ($F_{(2,198)} = 3.58$; $p < 0.05$). Reductions in dendritic length occurred throughout the radial distribution in SCI + vehicle animals, compared to sham animals (an average of 23.6%, 0–300 degrees; $F_{(1,132)} = 15.64$; $p < 0.01$), with the largest reduction occurring ventromedially (300–360 degrees; 38.9%); however, the group × location interaction did not reach significance ($F_{(11,132)} = 1.67$; $p = 0.086$). Treatment with ATK attenuated SCI-induced reductions in dendritic length per bin throughout the radial distribution and there were no group differences ($F_{(1,143)} = 0.14$, n.s.) and no group × location interaction ($F_{(11,143)} = 0.69$, n.s.) between SCI + ATK and sham animals. Dendritic lengths per bin in SCI + ATK animals were longer than those of SCI + vehicle animals throughout the radial distribution ($F_{(1,121)} = 4.44$; $p < 0.05$); there was no group × location interaction ($F_{(11,121)} = 0.70$, n.s.).

To definitively determine the role of cPLA₂ in dendritic atrophy after SCI, we used cPLA₂$^{-/-}$ mice and compared them to WT littermates (cPLA₂$^{+/+}$). Dendritic length decreased by 24.61% (3017.13 ± 361.67 µm in WT SCI animals, compared to 4002.23 ± 193.64 µm in sham animals). cPLA₂ deletion attenuated SCI-induced dendritic atrophy: Dendritic lengths in cPLA₂ KO mice were 3766.44 ± 325.74 µm, which were 24.84% longer than those of WT animals. These differences in dendritic lengths across groups approached statistical significance ($F_{(2,21)} = 2.89$; $p = 0.077$; Fig. 3D).

Dendritic length per bin was nonuniform across radial bins, and a repeated-measures ANOVA revealed a significant effect of radial location ($F_{(11,231)} = 27.49$; $p < 0.05$; Fig. 3E). Consistent with the results of the arbor per cell analysis, the effect of group was significant ($F_{(2,231)} = 4.95$; $p < 0.05$), with reductions in dendritic length occurring throughout the radial distribution in WT SCI animals, compared to sham animals (an average of 22.15%); there was no significant group × location interaction ($F_{(22,231)} = 1.07$, n.s.). cPLA₂ deletion attenuated SCI-induced reductions in dendritic length per bin, and there were no group differences ($F_{(1,154)} = 1.32$, n.s.) and no group × location interaction ($F_{(1,154)} = 0.42$, n.s.) between SCI cPLA₂ KO animals and sham animals. Dendritic lengths per bin in cPLA₂ KO animals were longer than those of WT animals after SCI throughout the radial distribution (an average of 35.53%), but this difference failed to reach statistical significance ($F_{(1,154)} = 3.30$; $p = 0.09$). There was no group × location interaction ($F_{(11,154)} = 1.03$, n.s.).

Dendritic extent

Consistent with the nonuniform dendritic distribution of quadriceps motoneurons apparent in Figure 2, radial dendritic extent differed across bins (Fig. 3C), and repeated-measures ANOVA revealed a significant effect of location ($F_{(11,198)} = 40.39$; $p < 0.0001$). However, radial dendritic extent did not differ across groups ($F_{(2,198)} = 3.26$, n.s.). Rostrocaudal dendritic extent also did not differ across groups ($F_{(2,18)} = 1.11$, n.s.), spanning 3220.00 ± 231.15 µm in sham animals, 2853.33 ± 186.67 µm in SCI + vehicle animals, and 2811.43 ± 223.17 µm in SCI + ATK animals. In cPLA₂ KO mice, consistent with the nonuniform dendritic distribution of quadriceps motoneurons, radial dendritic extent differed across bins, and repeated-measures ANOVA revealed a significant effect of location ($F_{(11,231)} = 62.26$; $p < 0.05$; Fig. 3F). However, radial dendritic extent did not differ across groups ($F_{(2,231)} = 3.14$, n.s.; Fig. 3F). Rostrocaudal dendritic extent also did not differ across groups ($F_{(2,21)} = 1.97$, n.s.), spanning 3220.00 ± 231.15 µm in sham animals, 2680.00 ± 156.39 µm in SCI WT animals, and 2740.00 ± 235.07 µm in cPLA₂ KO SCI animals.

Muscle weight and fiber size

Overall body weight was not affected: Animals weighed an average of 19.96 ± 0.38 g at end of treatment, and this did not differ between groups ($F_{(2,19)} = 2.44$, n.s.). However, muscle weights were affected by contusion injury (Fig. 4B). Weights of the vastus lateralis muscles decreased by 28.2% (0.05 ± 0.003 g in SCI +
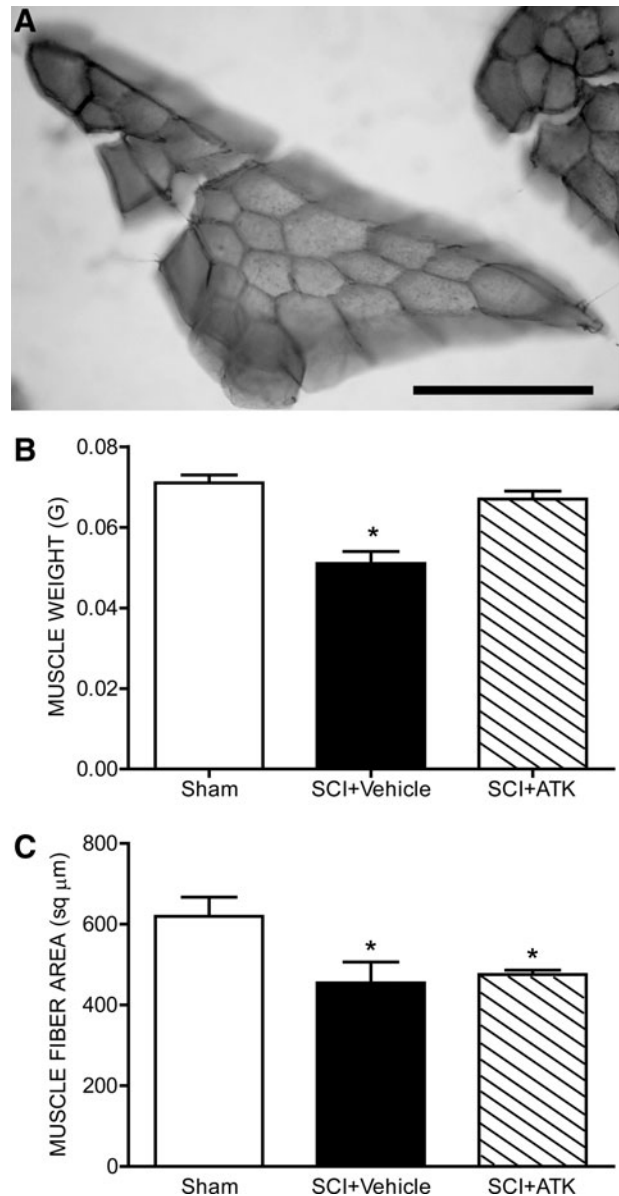

FIG. 4. Histological and morphological analysis of the vastus lateralis muscle after contusive spinal cord injury (SCI) with or without treatment. (**A**) Representative cross-section through the body of the vastus lateralis muscle from a sham animal stained with Milligan's trichrome stain. Weights (**B**) and cross-sectional fiber areas (**C**) of the vastus lateralis muscles in sham animals and injured animals that were either untreated (SCI + vehicle) or treated with arachidonyl trifluoromethyl ketone (ATK; SCI + ATK). After contusion injury, both the weight and fiber size of the vastus lateralis muscle in untreated animals were reduced over 20%. Treatment with ATK attenuated reductions in weight, but not fiber area. Bar heights represent means ± standard error of the mean. *Significantly different from sham animals. Scale bar, 100 µm.
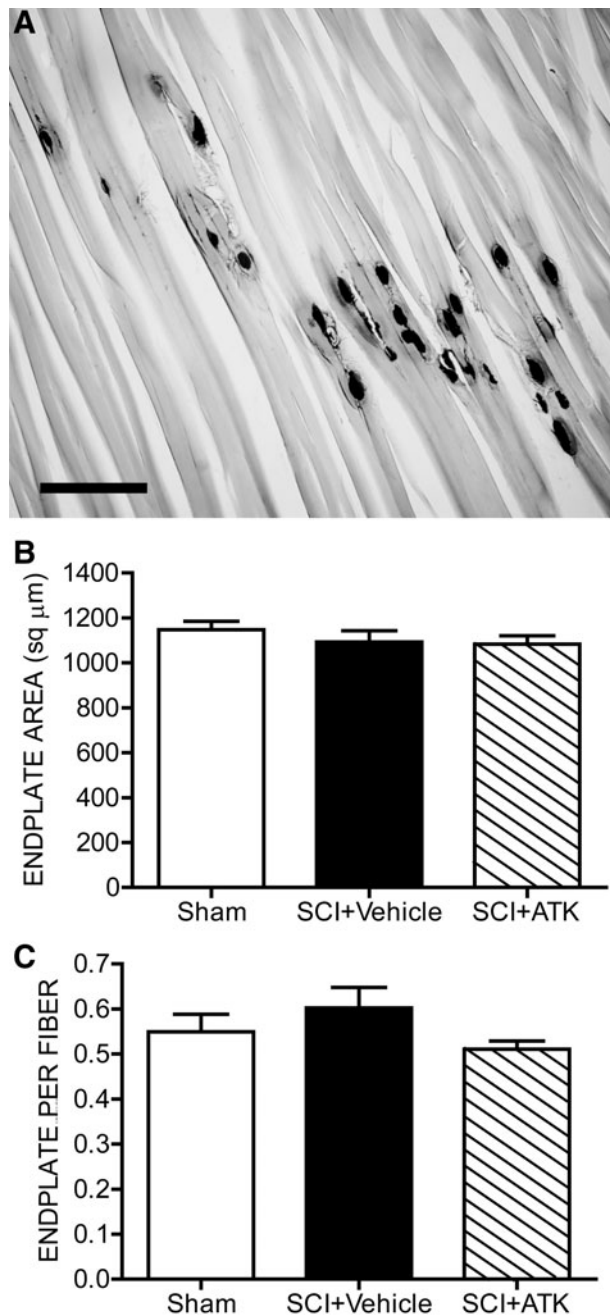
FIG. 5. Histological and morphological analysis of motor endplate size after contusive spinal cord injury (SCI) with or without treatment. (**A**) Representative longitudinal section through the body of the vastus lateralis muscle from a sham animal after staining for acetylcholinesterase. SCI had no effect on the motor endplate size (**B**) or density (**C**), regardless of treatment. Bar heights represent means ± standard error of the mean. Scale bar, 250 μm. ATK, arachidonyl trifluoromethyl ketone.

vehicle animals, compared to 0.071 ± 0.002 g for sham animals; LSD, $p < 0.0001$; overall test for the effect of group on muscle weight, $F_{(2,19)} = 17.81$; $p < 0.0001$). However, treatment with ATK attenuated SCI-induced muscle atrophy: Weights of the vastus lateralis muscles in SCI + ATK animals (0.067 ± 0.002 g) were 31.4% larger than those of SCI + vehicle animals (LSD, $p < 0.0001$) and did not differ from those of sham animals (LSD, n.s.).

Muscle fiber size was also affected by contusion injury (Fig. 4C). Cross-sectional area of vastus lateralis muscle fibers decreased by 26.6% (454.53 ± 51.63 μm² in SCI + vehicle animals, compared to 619.28 ± 47.72 μm² for sham animals; LSD, $p < 0.05$; overall test for the effect of group on muscle fiber area, $F_{(2,18)} = 5.56$; $p < 0.05$). However, treatment with ATK failed to attenuate SCI-induced muscle fiber size: Cross-sectional areas of vastus lateralis muscle fibers in SCI + ATK animals (475.50 ± 10.38 μm²) were not different from those of SCI + vehicle animals (LSD, n.s.) and were 23.2% smaller than those of sham animals (LSD, $p < 0.05$).

Motor endplate size and density

Contusion injury with or without ATK treatment had no significant effects on motor endplate size. In sham animals, motor endplate areas were typical in size (1147.92 ± 36.71 μm²) and did not differ from those of SCI + vehicle (1092.02 ± 50.40 μm²) or SCI + ATK animals (1083.69 ± 36.57 μm²; $F_{(2,19)} = 0.80$, n.s.; Fig. 5B). Similarly, the density of motor endplates did not differ across groups (sham animals, 0.55 ± 0.04 endplates per fiber; SCI + vehicle animals, 0.60 ± 0.05 endplates per fiber; SCI + ATK animals, 0.51 ± 0.04 endplates per fiber; $F_{(2,18)} = 1.44$, n.s.; Fig. 5C).

Discussion

In this study, we found that ATK treatment can completely prevent pronounced dendritic atrophy in spinal motoneurons caudal to a contusive SCI, indicating a protective role of cPLA$_2$ inhibition on prevention of motoneuron dendritic degeneration after SCI. Genetic deletion of cPLA$_2$ significantly reduced dendritic atrophy after SCI. It should be noted that, after SCI, motoneurons caudal to the injury are morphologically intact and are not directly traumatized by the injury. Inhibition of cPLA$_2$ also prevented decreases in weights of the target musculature. To our knowledge, this is the first study demonstrating a neuroprotective effect of cPLA$_2$ inhibition on motoneuron dendritic degenerative change and muscle morphology after SCI. Such injury-induced secondary effect on motoneurons and associated musculature remote to the injury itself may provide new targets for therapeutical interventions aimed at enhancing recovery of function after SCI.

Cytosolic phospholipase A$_2$ inhibition as a neuroprotective strategy

Mouse SCI models are being increasingly used because transgenic and KO mice are available for the study of cellular mechanisms. Certain mouse strains, such as C57BL/6, 129/Sv, and B10.rIII, have a naturally occurring null mutation of the major form of sPLA$_2$.[40] Therefore, C57BL/6 mice in this study were deficient in sPLA$_2$. ATK is a potent, selective inhibitor of cPLA$_2$. This inhibitor shows slow, tight binding to cPLA$_2$ in the presence of Ca^{2+} and forms a covalent bond with a serine residue in the active site of the enzyme.[19,41] This inhibitor is approximately 500-fold more potent at inhibiting cPLA$_2$ than sPLA$_2$[19] and may also be a weak inhibitor of iPLA$_2$.[42–44]

After contusion, the focal injuries delivered to the spinal cord developed into large lesions that spanned multiple thoracic spinal segments. Such lesions were significantly reduced by ATK treatment. Notably, the cPLA$_2$ inhibitor was administered after trauma, modeling a clinically relevant situation. These findings are in agreement with our previous studies that inhibition of PLA$_2$ reduced tissue damage and increased spared WM after SCI.[7,13] Several other studies also reported a detrimental effect of cPLA$_2$ in other central nervous

system diseases, such as ischemia,[45,46] experimental autoimmune encephalomyelitis,[20,47] and Alzheimer's disease.[48]

Our previous studies showed that SCI significantly induced cPLA₂ activation, which was observed as early as 8 h postinjury and peaked at 7 days postinjury. Activated cPLA₂ was mainly localized in neurons and oligodendrocytes. It has also been shown that AA and eicosanoids, downstream metabolites of cPLA₂, increased as early as 30 min after SCI.[49,50] The increased eicosanoids were persistent for at least 3 days (the longest time point studied) after SCI.[51] In addition, concentrations of free FA quickly increased after SCI, peaked at 3 days, and remained significantly high at 7 days after SCI.[52] Given that induction profiles of these PLA₂ metabolites are similar to that of cPLA₂ after SCI, a prolonged effect of cPLA₂ after SCI exists, suggesting that there might be a unique ''therapeutic window'' for intervention. Although cPLA₂ inhibitor in the present study was administered for 2 weeks after trauma, the optimal therapeutic time window for such treatment remains to be determined.

Changes in motoneuron morphology are not direct effects of lesion

Although extensive, spinal lesions did not extend into the lumbar spinal cord, thus sparing the GM and resident motoneurons. Counts of either Nissl-stained or BHRP-labeled motoneurons in SCI animals did not differ from those of sham animals, confirming that quadriceps motoneurons were not directly damaged by the initial trauma or secondary degeneration that occurred at the lesion site. Similarly, soma size of quadriceps motoneurons was not significantly affected by SCI, further suggesting that the quadriceps motoneurons were not directly damaged by the SCI.[5]

Dendritic atrophy after spinal cord injury

Afferent input to motoneurons is important for maintenance of dendritic morphology, and deafferentation often results in dendritic retraction. After deafferentation though damage to the dorsal horn,[53] spinal cord hemisection or transection,[35,54] or cortical ablation,[55] spinal motoneurons undergo dendritic atrophy. Activity in afferent pathways is an important factor in maintaining dendritic morphology. For example, cold block of the spinal cord causes dendritic morphological changes to develop within 4 h.[56] We have previously reported that, after SCI and the concomitant loss of descending pathways, spinal motoneurons caudal to the lesion undergo marked reductions in their dendritic arbor, especially ventromedially in areas where both the reticulo- and propriospinal projections terminate.[5] In the present study, we observed reductions throughout the arbor, but, again, the reductions were greatest in the ventromedial portion of the dendritic distribution. This loss is of particular significance after SCI, given that descending reticulospinal fibers course through the ventral and lateral funiculi,[57,58] and disruption of these tracts results in hindlimb motor deficits.[59,60] Therefore, it is possible that the dendritic atrophy we observed after SCI in untreated animals could reflect deafferentation resulting from loss of descending motor and propriospinal tracts.

Inhibition of cytosolic phospholipase A₂ attenuates spinal cord injury–induced motoneuron dendritic atrophy

SCI-induced atrophy of quadriceps motoneuron dendrites was attenuated in ATK-treated animals. Genetic deletion of cPLA₂ also resulted in neuroprotection on dendritic atrophy after SCI. However, mechanisms of cPLA₂ inhibition-mediated motoneuron atrophy remain unclear. One possibility is that ATK treatment could

have attenuated dendritic atrophy by increasing the number of spared axons that traverse the lesion, which is consistent with the reduction in lesion size and corresponding increase in WM sparing. The other possibility is that cPLA₂ may have a direct effect on dendrites. Such a direct effect is supported by other reports that cPLA₂ activation mediates Sema3A-induced growth cone collapse,[16,17] suggesting that cPLA₂ activation could be directly involved in dendritic retraction after SCI. The attenuation in dendritic atrophy we observed in ATK-treated animals could potentially maintain motor activation and account for the protective effects of ATK on locomotor function we have observed.[13] Such an effect would lead to protection of the target musculature from disuse atrophy and could support exercise training effects on locomotor function after SCI.[61,62]

Comparability of horseradish peroxidase conjugated to the cholera toxin B subunit labeling

We believe that the differences we observed across treatment groups reflect true dendritic atrophy in quadriceps motoneurons of untreated SCI animals, which is attenuated by treatment with ATK. However, the possibility that confounding changes arising from SCI could affect retrograde transport is an important consideration, given that such an artifact could potentially result in apparent alterations in dendritic morphology. However, no differences in either radial or rostrocaudal extents of quadriceps motoneuron dendrites in SCI groups, compared to normal values, were observed. Therefore, we believe that the dendritic labeling across groups was comparable and that the shorter dendritic lengths we observed in untreated SCI animals reflect true dendritic atrophy.

Muscle atrophy after spinal cord injury

The regressive changes we observed in muscle weight and fiber diameter are typical after SCI in muscles innervated by motoneurons below the level of the lesion, especially in weight-bearing muscles, such as the quadriceps.[63,64] This atrophy can result from either denervation owing to loss of motoneurons or damage to the ventral roots, or disuse consequent to decreases in muscle activation potentially owing to loss of synaptic input to remaining motoneurons.[65] In the current study, the atrophy we observed cannot be ascribed to an effect of denervation, given that we observed no changes in quadriceps motoneuron number, the number of BHRP-labeled quadriceps motoneurons, or the sizes or densities of motor endplates between sham animals and untreated SCI animals. Thus, the decreased weight and fiber size we observed most likely reflect a disuse atrophy, potentially resulting after damage to descending and propriospinal projections and/or reductions in quadriceps motoneuron dendritic length we observed. Such reductions in quadriceps motoneuron dendritic length result in attenuation of motor activation, reducing response amplitudes in the femoral nerve generated by dorsal root afferent stimulation.[6] Alternatively, disuse atrophy may also result from changes in muscle length or loading conditions that could decrease protein synthesis and increase protein degradation.[66,67]

Protection of muscle with arachidonyl trifluoromethyl ketone

In the current study, ATK treatment prevented atrophy in muscle weight observed after SCI. However, there is no significant difference in muscle fiber area between the SCI and SCI + ATK treatment groups. The reason for the reversal of muscle weight loss without changing of muscle fiber size is unclear. The protection of

muscle weight could be the result of a sparing of motoneuron function. As described above, ATK treatment can reverse the regressive changes in dendritic morphology and motor activation. Thus, the protection from dendritic atrophy with ATK treatment after SCI could have spared local spinal circuitry sufficiently to maintain motor activation and use legs more for walking, preventing disuse atrophy of target muscles.

Conclusions

The present results indicate that the regressive changes in motoneuron and muscle morphology observed after SCI can be prevented by blocking cPLA$_2$ pharmacologically at 30 min postinjury or genetically deleting cPLA$_2$ in mice, potentially providing a mechanism for the improved locomotor performance previously observed with cPLA$_2$ inhibitor treatments after SCI. Together, these results further support a role for cPLA$_2$ as a therapeutic target for treatment of SCI.

Funding Statement

Author Disclosure Statement

No competing financial interests exist.

References

1. Doherty, J.G., Burns, A.S., O'Ferrall, D.M., and Ditunno, J.F., Jr. (2002). Prevalence of upper motor neuron vs lower motor neuron lesions in complete lower thoracic and lumbar spinal cord injuries. J. Spinal Cord Med. 25, 289–292.

2. Liu, D., Thangnipon, W., and McAdoo, D.J. (1991). Excitatory amino acids rise to toxic levels upon impact injury to the rat spinal cord. Brain Res. 547, 344–348.

3. Diaz-Ruiz, A., Ibarra, A., Perez-Severiano, F., Guizar-Sahagun, G., Grijalva, I., and Rios, C. (2002). Constitutive and inducible nitric oxide synthase activities after spinal cord contusion in rats. Neurosci. Lett. 319, 129–132.

4. Ritz, M.F., and Hausmann, O.N. (2008). Effect of 17beta-estradiol on functional outcome, release of cytokines, astrocyte reactivity and inflammatory spreading after spinal cord injury in male rats. Brain Res. 1203, 177–188.

5. Byers, J.S., Huguenard, A.L., Kuruppu, D., Liu, N.K., Xu, X.M., and Sengelaub, D.R. (2012). Neuroprotective effects of testosterone on motoneuron and muscle morphology following spinal cord injury. J. Comp. Neurol. 520, 2683–2696.

6. Little, C.M., Coons, K.D., and Sengelaub, D.R. (2009). Neuroprotective effects of testosterone on the morphology and function of somatic motoneurons following the death of neighboring motoneurons. J. Comp. Neurol. 512, 359–372.

7. Liu, N.K., Zhang, Y.P., Han, S., Pei, J., Xu, L.Y., Lu, P.H., Shields, C.B., and Xu, X.M. (2007). Annexin A1 reduces inflammatory reaction and tissue damage through inhibition of phospholipase A2 activation in adult rats following spinal cord injury. J. Neuropathol. Exp. Neurol. 66, 932–943.

8. Liu, N.K., Zhang, Y.P., Titsworth, W.L., Jiang, X., Han, S., Lu, P.H., Shields, C.B., and Xu, X.M. (2006). A novel role of phospholipase A2 in mediating spinal cord secondary injury. Ann. Neurol. 59, 606–619.

9. Farooqui, A.A., Yang, H.C., Rosenberger, T.A., and Horrocks, L.A. (1997). Phospholipase A2 and its role in brain tissue. J. Neurochem. 69, 889–901.

10. Farooqui, A.A., Litsky, M.L., Farooqui, T., and Horrocks, L.A. (1999). Inhibitors of intracellular phospholipase A2 activity: their neurochemical effects and therapeutical importance for neurological disorders. Brain Res. Bull. 49, 139–153.

11. Liu, N.K., and Xu, X.M. (2010). Phospholipase A2 and its molecular mechanism after spinal cord injury. Mol. Neurobiol. 41, 197–205.

12. Bonventre, J.V. (1996). Roles of phospholipases A2 in brain cell and tissue injury associated with ischemia and excitotoxicity. J. Lipid Mediat. Cell Signal. 14, 15–23.

13. Liu, N.K., Deng, L.X., Zhang, Y.P., Lu, Q.B., Wang, X.F., Hu, J.G., Oakes, E., Bonventre, J.V., Shields, C.B., and Xu, X.M. (2014). Cytosolic phospholipase A protein as a novel therapeutic target for spinal cord injury. Ann. Neurol. 75, 644–658.

14. Murakami, M., Nakatani, Y., Atsumi, G., Inoue, K., and Kudo, I. (1997). Regulatory functions of phospholipase A2. Crit. Rev. Immunol. 17, 225–283.

15. Clark, J.D., Schievella, A.R., Nalefski, E.A., and Lin, L.L. (1995). Cytosolic phospholipase A2. J. Lipid Mediat. Cell Signal. 12, 83–117.

16. Sanford, S.D., Yun, B.G., Leslie, C.C., Murphy, R.C., and Pfenninger, K.H. (2012). Group IVA phospholipase A(2) is necessary for growth cone repulsion and collapse. J. Neurochem. 120, 974–984.

17. Mikule, K., Gatlin, J.C., de la Houssaye, B.A., and Pfenninger, K.H. (2002). Growth cone collapse induced by semaphorin 3A requires 12/15-lipoxygenase. J. Neurosci. 22, 4932–4941.

18. Harrison, M., O'Brien, A., Adams, L., Cowin, G., Ruitenberg, M.J., Sengul, G., and Watson, C. (2013). Vertebral landmarks for the identification of spinal cord segments in the mouse. Neuroimage 68, 22–29.

19. Street, I.P., Lin, H.K., Laliberte, F., Ghomashchi, F., Wang, Z., Perrier, H., Tremblay, N.M., Huang, Z., Weech, P.K., and Gelb, M.H. (1993). Slow- and tight-binding inhibitors of the 85-kDa human phospholipase A2. Biochemistry 32, 5935–5940.

20. Kalyvas, A., and David, S. (2004). Cytosolic phospholipase A2 plays a key role in the pathogenesis of multiple sclerosis-like disease. Neuron 41, 323–335.

21. Fargo, K.N., and Sengelaub, D.R. (2004). Testosterone manipulation protects motoneurons from dendritic atrophy after contralateral motoneuron depletion. J. Comp. Neurol. 469, 96–106.

22. Fargo, K.N., and Sengelaub, D.R. (2004). Exogenous testosterone prevents motoneuron atrophy induced by contralateral motoneuron depletion. J. Neurobiol. 60, 348–359.

23. Fargo, K.N., and Sengelaub, D.R. (2007). Androgenic, but not estrogenic, protection of motoneurons from somal and dendritic atrophy induced by the death of neighboring motoneurons. Dev. Neurobiol. 67, 1094–1106.

24. Goldstein, L.A., Kurz, E.M., and Sengelaub, D.R. (1990). Androgen regulation of dendritic growth and retraction in the development of a sexually dimorphic spinal nucleus. J. Neurosci. 10, 935–946.

25. Kurz, E.M., Sengelaub, D.R., and Arnold, A.P. (1986). Androgens regulate the dendritic length of mammalian motoneurons in adulthood. Science 232, 395–398.

26. Michel, R.P., and Cruz-Orive, L.M. (1988). Application of the Cavalieri principle and vertical sections method to lung: estimation of volume and pleural surface area. J. Microsc. 150, 117–136.

27. Oorschot, D.E. (1994). Are you using neuronal densities, synaptic densities or neurochemical densities as your definitive data? There is a better way to go. Prog. Neurobiol. 44, 233–247.

28. Nicolopoulos-Stournaras, S., and Iles, J.F. (1983). Motor neuron columns in the lumbar spinal cord of the rat. J. Comp. Neurol. 217, 75–85.

29. Brushart, T.M., and Seiler, W.A., 4th. (1987). Selective reinnervation of distal motor stumps by peripheral motor axons. Exp. Neurol. 97, 289–300.

30. Al-Majed, A.A., Brushart, T.M., and Gordon, T. (2000). Electrical stimulation accelerates and increases expression of BDNF and trkB mRNA in regenerating rat femoral motoneurons. Eur. J. Neurosci. 12, 4381–4390.

31. Gundersen, H.J. (1988). The nucleator. J. Microsc. 151, 3–21.

32. Kurz, E.M., Brewer, R.G., and Sengelaub, D.R. (1991). Hormonally mediated plasticity of motoneuron morphology in the adult rat spinal cord: a cholera toxin-HRP study. J. Neurobiol. 22, 976–988.

33. Goldstein, L.A., Kurz, E.M., Kalkbrenner, A.E., and Sengelaub, D.R. (1993). Changes in dendritic morphology of rat spinal motoneurons during development and after unilateral target deletion. Brain Res. Dev. Brain Res. 73, 151–163.

34. Goldstein, L.A., and Sengelaub, D.R. (1994). Differential effects of dihydrotestosterone and estrogen on the development of motoneuron morphology in a sexually dimorphic rat spinal nucleus. J. Neurobiol. 25, 878–892.

35. Hebbeler, S.L., and Sengelaub, D.R. (2003). Development of a sexually dimorphic neuromuscular system in male rats after spinal transection: morphologic changes and implications for estrogen sites of action. J. Comp. Neurol. 467, 80–96.

36. Hebbeler, S.L., Verhovshek, T., and Sengelaub, D.R. (2002). N-methyl-D-aspartate receptor blockade inhibits estrogenic support of dendritic growth in a sexually dimorphic rat spinal nucleus. J. Comp. Neurol. 451, 142–152.

37. Kalb, R.G. (1994). Regulation of motor neuron dendrite growth by NMDA receptor activation. Development 120, 3063–3071.

38. Wilson, R.E., Coons, K.D., and Sengelaub, D.R. (2009). Neuroprotective effects of testosterone on dendritic morphology following partial motoneuron depletion: efficacy in female rats. Neurosci. Lett. 465, 123–127.

39. Hedreen, J.C., Bacon, S.J., and Price, D.L. (1985). A modified histochemical technique to visualize acetylcholinesterase-containing axons. J. Histochem. Cytochem. 33, 134–140.

40. Kennedy, B.P., Payette, P., Mudgett, J., Vadas, P., Pruzanski, W., Kwan, M., Tang, C., Rancourt, D.E., and Cromlish, W.A. (1995). A natural disruption of the secretory group II phospholipase A2 gene in inbred mouse strains. J. Biol. Chem. 270, 22378–22385.

41. Trimble, L.A., Street, I.P., Perrier, H., Tremblay, N.M., Weech, P.K., and Bernstein, M.A. (1993). NMR structural studies of the tight complex between a trifluoromethyl ketone inhibitor and the 85-kDa human phospholipase A2. Biochemistry 32, 12560–12565.

42. Riendeau, D., Guay, J., Weech, P.K., Laliberte, F., Yergey, J., Li, C., Desmarais, S., Perrier, H., Liu, S., Nicoll-Griffith, D., and Street, I. P. (1994). Arachidonyl trifluoromethyl ketone, a potent inhibitor of 85-kDa phospholipase A2, blocks production of arachidonate and 12-hydroxyeicosatetraenoic acid by calcium ionophore-challenged platelets. J. Biol. Chem. 269, 15619–15624.

43. Ackermann, E.J., Conde-Frieboes, K., and Dennis, E.A. (1995). Inhibition of macrophage Ca(2+)-independent phospholipase A2 by bromoenol lactone and trifluoromethyl ketones. J. Biol. Chem. 270, 445–450.

44. Ghomashchi, F., Loo, R., Balsinde, J., Bartoli, F., Apitz-Castro, R., Clark, J.D., Dennis, E.A., and Gelb, M.H. (1999). Trifluoromethyl ketones and methyl fluorophosphonates as inhibitors of group IV and VI phospholipases A(2): structure-function studies with vesicle, micelle, and membrane assays. Biochim. Biophys. Acta 1420, 45–56.

45. Bonventre, J.V., Huang, Z., Taheri, M.R., O'Leary, E., Li, E., Moskowitz, M.A., and Sapirstein, A. (1997). Reduced fertility and post-ischaemic brain injury in mice deficient in cytosolic phospholipase A2. Nature 390, 622–625.

46. Tabuchi, S., Uozumi, N., Ishii, S., Shimizu, Y., Watanabe, T., and Shimizu, T. (2003). Mice deficient in cytosolic phospholipase A2 are less susceptible to cerebral ischemia/reperfusion injury. Acta Neurochir. Suppl. 86, 169–172.

47. Marusic, S., Leach, M.W., Pelker, J.W., Azoitei, M.L., Uozumi, N., Cui, J., Shen, M.W., DeClercq, C.M., Miyashiro, J.S., Carito, B.A., Thakker, P., Simmons, D.L., Leonard, J.P., Shimizu, T., and Clark, J.D. (2005). Cytosolic phospholipase A2 alpha-deficient mice are resistant to experimental autoimmune encephalomyelitis. J. Exp. Med. 202, 841–851.

48. Sanchez-Mejia, R.O., Newman, J.W., Toh, S., Yu, G.Q., Zhou, Y., Halabisky, B., Cisse, M., Scearce-Levie, K., Cheng, I.H., Gan, L., Palop, J.J., Bonventre, J.V., and Mucke, L. (2008). Phospholipase A2 reduction ameliorates cognitive deficits in a mouse model of Alzheimer's disease. Nat. Neurosci. 11, 1311–1318.

49. Demediuk, P., Saunders, R.D., Anderson, D.K., Means, E.D., and Horrocks, L.A. (1987). Early membrane lipid changes in laminectomized and traumatized cat spinal cord. Neurochem. Pathol. 7, 79–89.

50. Demediuk, P., Saunders, R.D., Anderson, D.K., Means, E.D., and Horrocks, L.A. (1985). Membrane lipid changes in laminectomized and traumatized cat spinal cord. Proc. Natl. Acad. Sci. U. S. A. 82, 7071–7075.

51. Resnick, D.K., Nguyen, P., and Cechvala, C.F. (2001). Regional and temporal changes in prostaglandin E2 and thromboxane B2 concentrations after spinal cord injury. Spine J. 1, 432–436.

52. Demediuk, P., Daly, M.P., and Faden, A.I. (1989). Changes in free fatty acids, phospholipids, and cholesterol following impact injury to the rat spinal cord. J. Neurosci. Res. 23, 95–106.

53. Bernstein, J.J., and Standler, N.A. (1983). Dendritic alteration of rat spinal motoneurons after dorsal horn mince: computer reconstruction of dendritic fields. Exp. Neurol. 82, 532–540.

54. Bernstein, J.J., Wacker, W., and Standler, N. (1984). Spinal motoneuron dendritic alteration after spinal cord hemisection in the rat. Exp. Neurol. 83, 548–554.

55. Standler, N.A., and Bernstein, J.J. (1984). Dendritic alteration of spinal motoneurons after ablation of somatomotor cortex. Exp. Neurol. 83, 264–273.

56. Castro-Moure, F., and Goshgarian, H.G. (1997). Morphological plasticity induced in the phrenic nucleus following cervical cold block of descending respiratory drive. Exp. Neurol. 147, 299–310.

57. Jones, B.E., and Yang, T.Z. (1985). The efferent projections from the reticular formation and the locus coeruleus studied by anterograde and retrograde axonal transport in the rat. J. Comp. Neurol. 242, 56–92.

58. Martin, G.F., Vertes, R.P., and Waltzer, R. (1985). Spinal projections of the gigantocellular reticular formation in the rat. Evidence for projections from different areas to laminae I and II and lamina IX. Exp. Brain Res. 58, 154–162.

59. Magnuson, D.S., Trinder, T.C., Zhang, Y.P., Burke, D., Morassutti, D.J., and Shields, C.B. (1999). Comparing deficits following excitotoxic and contusion injuries in the thoracic and lumbar spinal cord of the adult rat. Exp. Neurol. 156, 191–204.

60. Loy, D.N., Talbott, J.F., Onifer, S.M., Mills, M.D., Burke, D.A., Dennison, J.B., Fajardo, L.C., Magnuson, D.S., and Whittemore, S.R. (2002). Both dorsal and ventral spinal cord pathways contribute to overground locomotion in the adult rat. Exp. Neurol. 177, 575–580.

61. Raineteau, O., and Schwab, M.E. (2001). Plasticity of motor systems after incomplete spinal cord injury. Nat. Rev. Neurosci. 2, 263–273.

62. Gazula, V.R., Roberts, M., Luzzio, C., Jawad, A.F., and Kalb, R.G. (2004). Effects of limb exercise after spinal cord injury on motor neuron dendrite structure. J. Comp. Neurol. 476, 130–145.

63. Peckham, P.H., Mortimer, J.T., and Marsolais, E.B. (1976). Alteration in the force and fatigability of skeletal muscle in quadriplegic humans following exercise induced by chronic electrical stimulation. Clin. Orthop. Relat. Res. (114), 326–333.

64. Giangregorio, L., and McCartney, N. (2006). Bone loss and muscle atrophy in spinal cord injury: epidemiology, fracture prediction, and rehabilitation strategies. J. Spinal Cord Med. 29, 489–500.

65. Gordon, T., and Mao, J. (1994). Muscle atrophy and procedures for training after spinal cord injury. Phys. Ther. 74, 50–60.

66. Goldspink, D.F. (1977). The influence of immobilization and stretch on protein turnover of rat skeletal muscle. J. Physiol. 264, 267–282.

67. Williams, P.E., and Goldspink, G. (1973). The effect of immobilization on the longitudinal growth of striated muscle fibres. J. Anat. 116, 45–55.

Address correspondence to:
Xiao-Ming Xu, MD, PhD
Stark Neurosciences Research Institute
Indiana University School of Medicine
320 West 15th Street
NB Room 500E
Indianapolis, IN 46202
USA

E-mail: xu26@iupui.edu